Cite this: *Biomater. Sci.*, 2020, **8**, 1951

Human fibroblast-macrophage tissue spheroids demonstrate ratio-dependent fibrotic activity for *in vitro* fibrogenesis model development†

Yu Tan,^{a,b} Allister Suarez,^{a,b} Matthew Garza,^{a,b} Aadil A. Khan,^{c,d} Jennifer Elisseeff ^b and Devin Coon *^{a,b}

Fibrosis is a pathological accumulation of excessive collagen that underlies many of the most common diseases, representing dysfunction of the essential processes of normal tissue healing. Fibrosis research aims to limit this response without ameliorating the essential role of fibrogenesis in organ function. However, the absence of a realistic *in vitro* model has hindered investigation into mechanisms and potential interventions because the standard 2D monolayer culture of fibroblasts has limited applicability. We sought to develop and optimize fibrosis spheroids: a scaffold-free three-dimensional human fibroblast-macrophage spheroid system representing an improved benchtop model of human fibrosis. We created, characterized and optimized human fibroblast-only spheroids, demonstrating increased collagen deposition compared to monolayer fibroblasts, while spheroids larger than 300 μm suffered from progressively increasing apoptosis. Next, we improved the spheroid system with the addition of human macrophages to more precisely recapitulate the environment during fibrogenesis, creating a hybrid spheroid system with different ratios of fibroblasts and macrophages ranging from 2 : 1 to 64 : 1. We found that in the hybrid spheroids (particularly the 16 : 1 [F16] ratio) more fibroblasts were activated, with greater macrophage polarization towards a pro-inflammatory M1 phenotype. Hybrid spheroids containing higher ratios of macrophages showed greater macrophage heterogeneity and less fibrogenesis, while low macrophage ratios limited macrophage-induced effects and yielded less collagen deposition. The F16 group also had the highest expression levels of fibrosis-related genes (*Col-1a1*, *Col-3a1* and *TGF- β*) and inflammation-related genes (*TNF*, *IL1 β* and *IL6*). IF staining demonstrated that F16 spheroids had the highest levels of αSMA , collagen-1 and collagen-3 deposition among all groups as well as formation of a dense collagen rim surrounding the spheroid. Future studies exploring the greater fibrotic activity of F16 spheroids may provide new mechanistic insights into diseases involving excessive fibrotic activity. Microtissue fibrosis models capable of achieving greater clinical fidelity have the potential to combine the relevance of animal models with the scale, cost and throughput of *in vitro* testing.

Received 10th June 2019,
Accepted 31st January 2020

DOI: 10.1039/c9bm00900k

rsc.li/biomaterials-science

Introduction

Fibrosis is a pathological accumulation of excessive collagen in tissues with attendant loss of function and considerable global disease burden.¹ Fibrosis underlies many disease states – pulmonary fibrosis, liver cirrhosis, myocardial infarction, renal

fibrosis, skin keloid, and others.^{2,3} Complications in the wound healing process, such as imbalance in the synthesis and breakdown of extracellular matrix proteins collagen 1 and 3, can lead to excessive scar tissue in fibrotic outcomes of keloids and hypertrophic scarring, respectively.^{4,5} In addition, local fibrosis can also impair normal functionality of the body such as in the foreign body response (FBR) around medical devices, which are surgically implanted into millions of patients each year. In response to implanted materials, the body initiates a fibrotic cascade and encapsulates the implant to separate it from the host environment. The FBR is an end-stage process that follows inflammation and wound healing around an implant in the body. It occurs on a spectrum from tissue ingrowth with minimal encapsulation to aggressive formation of a thick, often symptomatic collagenous capsule, mediated by a complex variety of factors including implant

^aDepartment of Plastic & Reconstructive Surgery, Johns Hopkins University School of Medicine, Baltimore, Maryland, USA

^bTranslational Tissue Engineering Center, Department of Biomedical Engineering, Johns Hopkins University Whiting School of Engineering, Baltimore, Maryland, USA

^cTargeted Therapy Team, Division of Radiotherapy and Imaging, The Institute of Cancer Research, London SW3 6JB, UK

^dDepartment of Plastic Surgery, The Royal Marsden Hospital, London SW3 6JJ, UK

†Electronic supplementary information (ESI) available. See DOI: 10.1039/c9bm00900k

material, surface properties, patient characteristics and more. The fibrous tissue that forms around the implant is distinguished by foreign body giant cells, fibroblasts, and macrophages.^{6–9} Fibrosis research often aims to identify clinically relevant methods to screen prophylactic agents and identify therapeutic targets that prevent aberrant scarring.⁴

The classical *in vitro* model for fibrogenesis mainly focuses on 2D monolayer cell culture of fibroblasts and is used for drug screening and development.^{4,10} However, cells cultured in a 2D environment are different in both physiology and in their cellular responses compared with cells *in vivo*.¹¹ As one example, current understanding of the fibrotic response to implanted devices suffers from a lack of generalizability—many factors (shape, material, *etc.*) impact FBR but there are too many permutations for *in vivo* testing to provide mechanistic insight. A more physiologically relevant *in vitro* fibrosis model can allow testing of the effect of each factor, alone and in combination, as well as mechanistic study (*e.g.*, signaling pathways) on a scale that is not feasible in animals. Thus, a better *in vitro* model is urgently needed for efficient drug testing and medical device design. In the past two decades, spheroids (scaffold-free spherical microtissues) have emerged in cancer research,^{12–14} tissue engineering,¹⁵ and cell therapy¹⁶ as a model that more closely mimics an *in vivo* environment with more representative cell–cell interactions and intercellular communication. Spheroids have been shown to have advantages over 2D culture models, as they have an improvement in stable morphology and cell polarity. Extensive research has been done in spheroids as model systems for tumors. Spheroids composed of co-cultured cell types mimic physiological cell–cell interactions in tissues.¹⁷

Macrophages are a key effector cell in the fibrosis process. Their effect in driving fibrosis through upregulation of fibroblast activation and collagen production has been known for many years. More recent studies have begun to elucidate much greater complexity to the role of macrophages, including subpopulations with different effects on inflammation and fibrosis (the M1/M2 spectrum).¹⁸ In addition, the modulation of pro-fibrotic macrophage activity by a complex range of signals, including cell–cell interactions with other macrophages and fibroblasts as well as two-way communication with other components of the immune system has increasingly been recognized.^{19–22}

In this work we sought to develop and optimize a scaffold-free three-dimensional spheroid system as an improved *in vitro* model of human fibrosis. We improved the spheroid system with the addition of an optimized ratio of human macrophages as effector cells to more precisely mimic the physiologic microenvironment during fibrogenesis, creating a hybrid spheroid system with improved performance compared to fibroblasts-only spheroids.

Methods

Primary human fibroblast cell culture

Johns Hopkins IRB approval was obtained for sample collection from surgical procedures. Human primary fibroblasts

(HFB) were obtained from clinical samples and cultured in DMEM with high glucose supplemented with 10% FBS and 1% Antibiotic–Antimycotic (Thermo Scientific, Pittsburgh, PA).²³ Briefly, tissue samples were placed in PBS supplemented with 5% Antibiotic–Antimycotic for 30 minutes. Then, specimens were minced, and the tissue fragments were seeded in T75 tissue culture flasks and suspended in fibroblast growth medium in the incubator. The outgrowth of fibroblasts from tissue fragments occurred after 1-week culture. When 80% confluency of fibroblasts was observed, the cells were detached with 0.25% trypsin-EDTA (Thermo Scientific, Pittsburgh, PA) and reseeded. Passage 2 or 3 of these human primary fibroblast cell lines were used in the following experiments.

Isolation of human monocytes and their differentiation into macrophages

Human monocytes were isolated from venous blood samples by density gradient centrifugation method.²⁴ Briefly, the diluted blood with cold PBS was layered on Ficoll-Paque Plus (GE Healthcare, Chicago, IL) in the ratio of 1 : 1 and subjected to centrifugation at 400g for 30 minutes at room temperature. The buffy-coat fraction (white layer) representing PBMCs was aspirated out gently and transferred into centrifuge tubes. The suspension of cells was then washed and cultured in RPMI 1640 (Thermo Scientific, Pittsburgh, PA) supplemented with 1% penicillin–streptomycin (Thermo Scientific, Pittsburgh, PA) and 10% heat-inactivated autologous human fibrin-depleted serum. After overnight incubation at 37 °C, non-adherent cells (lymphocytes) were removed by flushing with fresh medium. We adopted a previously reported differentiation protocol which has been shown to produce an uncommitted macrophage phenotype.^{25,26} The adherent monocytes were cultured continuously for 2 weeks to yield differentiated human macrophages (HM) with both M1 and M2 phenotypes,^{24,27} as shown in ESI Fig. 2.†

Spheroid fabrication

Fibroblast-only or hybrid spheroids were fabricated in non-adhesive agarose hydrogel molds.²⁸ The agarose molds were casted using Mold Master (Microtissues, Inc., Providence, RI, USA) as negative replicates to create molds containing 35 concave recesses with hemispheric bottoms (800 μm diameter, 800 μm deep) to facilitate the formation of cell spheroids. Next, 330 μl of 2% autoclaved agarose solution was pipetted into the Mold Master, carefully detached after gelation at room temperature, and transferred into one well of 12-wells culture plate. A volume of 75 μl of the cell suspension with different concentrations was pipetted into each agarose mold. After the cells settled into the recesses of the mold (15 min), additional media was added (2 ml) and exchanged every 2 days for the length of the experiment. In co-cultured spheroids composed of fibroblasts and macrophages, cell suspensions were prepared with each cell type and counted prior to mixing them in the desired ratios. Briefly, 0.6×10^6 cells per ml was prepared for fibroblast and macrophage cell suspensions, respectively. A 75 μl cell mixture of these two cell types was prepared in

accordance to the different ratios (fibroblasts and macrophages 2:1 = 50 μ l:25 μ l, 4:1 = 60 μ l:15 μ l, 8:1 = 66.7 μ l:8.3 μ l, 16:1 = 70.6 μ l:4.4 μ l, 32:1 = 72.7 μ l:2.3 μ l, 64:1 = 73.8 μ l:1.2 μ l, 100:0 = 75 μ l:0 μ l) and subsequently pipetted into the agarose molds (ESI Fig. 1†).

Genes expression analysis with qRT-PCR

RNA was extracted from monolayers (0.1 million cells) or spheroids (35 spheroids) with a RNeasy Kit following manufacturer's instructions (Qiagen, Valencia, CA). Total RNA was quantified with a NanoDrop 2000c (NanoDrop, Wilmington, DE) and 2 μ g of total RNA was retro-transcribed with a Superscript VILO cDNA Synthesis Kit (Life Technologies, Carlsbad, CA) for cDNA synthesis according to the manufacturer's protocol. Quantitative real-time polymerase chain reaction (qRT-PCR) was performed and monitored using the SYBR Green PCR Mastermix (Life Technologies, Carlsbad, CA) on the StepOnePlus Real Time PCR System (Life Technologies, Carlsbad, CA). Reaction mixtures were incubated for 10 minutes at 95 °C followed by 40 cycles of 15 seconds at 95 °C, 1 minute at 60 °C, and finally 15 seconds at 95 °C, 1 minute at 60 °C, and 15 seconds at 95 °C. For each sample, gene expression was normalized to the level of GAPDH used as a housekeeping gene. All samples were run in duplicate. The level of expression of the target gene was calculated as $2^{-\Delta\Delta Ct}$ as previously described.²⁹

Immunofluorescent staining

Freshly collected spheroids were placed onto a cryomold (Sakura, Japan) and covered with OCT (Thermo Scientific, Pittsburgh, PA). The cryomold containing spheroids was immediately stored at -80 °C. Frozen spheroids were cryosectioned into 10 μ m thick layers onto glass slides for immunohistochemistry. The sections were fixed with precooled acetone (-20 °C) for 10 min. After washing (3 times at 5 min) in 1 \times PBS with 0.1% Triton X-100 (PBST), 100 μ l of blocking buffer was added (10% goat serum in 1 \times PBS) onto sections and incubated in a humidified chamber at room temperature for 1 h. Sections were incubated with appropriately diluted primary antibodies: Collagen-1 (Abcam, Cambridge, UK), Caspase-3 (Abcam, Cambridge, UK), alpha-smooth muscle actin (Millipore, Billerica, MA), Ki67 (Abcam, Cambridge, UK), Collagen-3 (Abcam, Cambridge, UK), HSP47 (Thermo Scientific, Pittsburgh, PA), CD68 (LSBio, Seattle, WA), CCR7 (Cell Signaling Technology, Danvers, MA) and pSTAT1 (Cell Signaling Technology, Danvers, MA) overnight at 4 °C. After washing in PBST (3 times at 5 min), tissues were incubated with fluorescent secondary antibodies diluted in PBST for 1 h at ambient temperature. After washing in PBST (3 times at 5 min), nuclei were stained with DAPI (Molecular Probes/Invitrogen, Eugene, OR) and diluted in PBST for 15 min at ambient temperature. Following the final washing procedure (PBST, 3 times at 5 min), glass cover slips were added to the slides using Fluoro-Gel (Electron Microscopy Sciences, Hatfield, PA). Immunostained samples were imaged with a

LSM510 laser scanning confocal microscope (Zeiss, Oberkochen, Germany).

Semi-quantitative analysis for immunofluorescent staining

We adopted a previously published and validated semi-quantitative method to analyze immunofluorescent stained images.^{28,30} Briefly, we used ImageJ software (National Institutes of Health, Bethesda, Maryland, USA) to measure the fluorescent signal area for each single channel slide on the spheroid cross section. The fluorescent signal area was divided by the total area of the spheroid to determine the 'covered area' percentage for each antibody staining on the spheroid ($N = 3$).

Statistical methods

Differences between experimental groups were analyzed using an independent student *t*-test and one-way ANOVA followed by Tukey's *post-hoc* test. $P < 0.05$ was considered significantly different for all statistical tests.

Results

Spheroid formation and effect of spheroid diameter on cellular viability and functionality

Human fibroblasts in a 3D scaffold-free spheroid system were successfully formed and cultured. They synthesized and deposited an abundant amount of ECM proteins such as collagen-1 after 7 days culture (Fig. 1A-E) to facilitate cellular assembly into spherical microtissue (spheroids) *in vitro*. In addition, the immunofluorescent staining of an apoptosis marker (Caspase-3) on cross-sections of the spheroid revealed that high-level viability of fibroblasts was observed for the spheroids with diameter less than 300 μ m (Fig. 1A-C) while significant cell apoptosis (Fig. 1D-F) was induced in spheroids with a larger size (≥ 400 μ m in diameter) due to progressive hypoxia in the core. Thus, we focused on spheroids with a diameter less than 300 μ m in the following experiments.

Characterization of HFB-only spheroid cellular phenotypes and gene expression

We collected bright-field images of the spheroids with 100 μ m, 200 μ m and 300 μ m diameters as shown in Fig. 2A-C at day 1, 5 and 7 post-fabrication. The statistics on diameter change over time (Fig. 2D-F) indicates the spheroids became denser over time, becoming mature in size after 5 days of culture in non-adhesive agarose hydrogel molds. H&E staining (Fig. 2G-I) was conducted to investigate the presence of necrosis and apoptotic cells in the spheroids. The results showed that there was no detectable necrosis or signs of apoptosis in the spheroids, which is consistent with Caspase-3 staining (Fig. 1A-C). In addition, the immunofluorescent staining (Fig. 2J-L) of proliferation marker (Ki67) suggests that the majority of fibroblasts maintained their proliferative phenotype while a few showed an activated myofibroblast phenotype with expression of alpha smooth muscle actin (α SMA). The qPCR data demon-

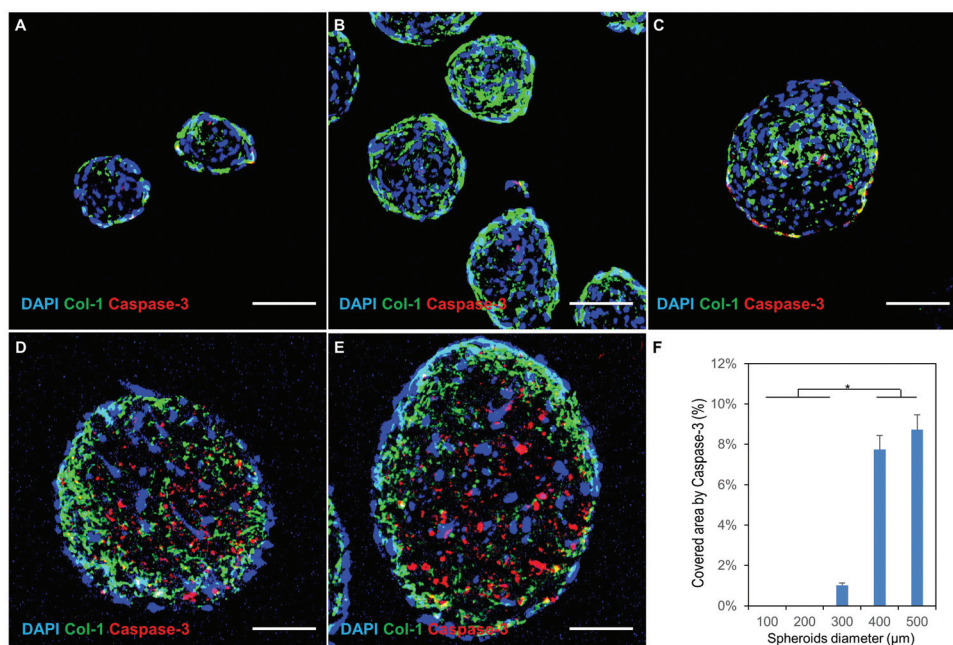


Fig. 1 Effect of spheroid size on cellular viability. (A–E) Confocal images of HFB spheroids with diameters of 100 μm , 200 μm , 300 μm , 400 μm and 500 μm respectively. Immunostaining for DAPI (nuclear marker); Col-1 (collagen type 1 synthesized by fibroblasts) and Caspase-3 (cell apoptosis). Significant hypoxia-induced cellular apoptosis is seen in the core of larger spheroids (400 μm and 500 μm in diameter). Scale bars: 100 μm . (F) Percentage of area positive for Caspase-3 in the cross-sectional imaging of the spheroids. ($n = 3$; $*p < 0.05$).

strated that fibroblasts in the 3D spheroids had significantly higher expression levels of fibrosis genes (αSMA and collagen-1) compared to the 2D monolayer culture used as control. The spheroids with 200 μm diameter showed the highest expression level of fibrosis genes among all groups due to significantly lower expression levels of matrix metalloproteinases genes such as MMP1, MMP2 and MMP7 (Fig. 2M–Q).

Creation and characterization of fibroblast-macrophage hybrid spheroids with optimization for modelling fibrosis

The absence of immune cell mediators was recognized as a likely limit to physiologic model behavior. In order to further mimic physiologic fibrosis, hybrid spheroids were fabricated with fibroblasts and macrophages in different ratios (2 : 1, 4 : 1, 8 : 1, 16 : 1, 32 : 1, 64 : 1 and 100 : 0 as control) based on the schematic (ESI Fig. 1†). Attempts at extremely high-macrophage spheroids (1 : 1 and 1 : 2 fibroblast : macrophage ratio) failed to form confluent 3D microtissue, potentially due to inadequate ECM secretion to support aggregation.

The immunofluorescent staining of a pan-macrophage marker³¹ confirmed that CD68 signal was reduced proportionally with each serial dilution that decreased the number of macrophages seeded into the spheroids (ESI Fig. 3 and 4A†). Hybrid spheroids with a 16 : 1 ratio (F16) consistently showed the highest expression level of collagen maturation marker (HSP47) among all groups (ESI Fig. 3B and 4†). The CD64 and CD68 (pan-macrophage) qPCR data (ESI Fig. 4B†) showed comparably preserved ratios of macrophage gene expression in spheroids.

The qPCR data was congruent with immunofluorescent stain results and confirmed that F16 had higher expression levels of fibrosis-related genes (Col-1a1, Col-3a1 and TGF- β) compared to the other hybrid spheroids and 100% fibroblast spheroids (Fig. 4). F16 hybrid spheroids also showed relatively lower expression levels of MMP7 (Fig. 4). In addition, F16 group demonstrated significantly higher expression levels of inflammation-related genes (TNF, IL1 β and IL6) among all the groups (Fig. 4).

Cell phenotype changes in hybrid spheroids regarding fibroblast activations and polarization of macrophages

Activated fibroblasts (myofibroblasts) and pro-inflammatory type M1 macrophages were identified in the hybrid spheroids by immunofluorescent staining of αSMA (Fig. 3 and ESI Fig. 7†) and CCR7/pSTAT1 (Fig. 5 and ESI Fig. 6†) respectively. This showed that some fibroblasts were activated as myofibroblasts. In addition, the F16 group showed the highest number of myofibroblasts and M1-type macrophages, potentially indicating higher fibrogenesis activity.

Collagen deposition in the hybrid spheroids as a fibrogenesis product

Abundant amounts of collagen deposition were observed in all hybrid spheroid and fibroblast-only groups, as shown in the immunofluorescent staining of collagen 1 and 3 in Fig. 6A. In addition, hybrid spheroids with high macrophage loads (2 : 1, 4 : 1 and 8 : 1) showed similar levels of collagen deposition compared with fibroblast-only spheroids, with more collagen

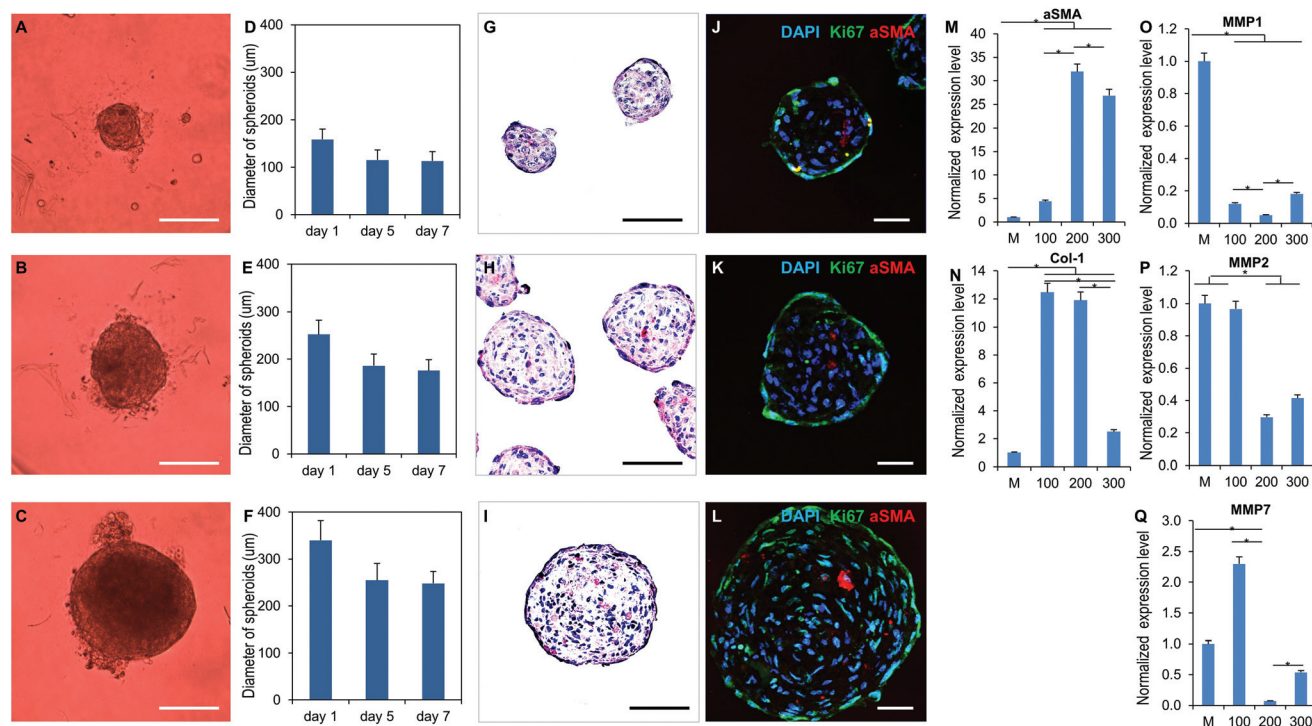


Fig. 2 Characterization of HFB spheroid morphology, phenotype and fibrosis-related gene expression. (A–C) Bright field images of HFB spheroids with diameters of 100 μm , 200 μm and 300 μm respectively. (D–F) Spheroids became dense and stable in size after 7 days of culture ($n = 12$, error bar represents standard deviation). (G–I) Bright field images of H&E staining of HFB spheroids with varying diameters. (J–L) Confocal images of HFBs spheroids show that some fibroblasts maintain proliferation capacity in spheroid form, with stains for DAPI (nuclei); αSMA (myofibroblasts) and Ki67 (cell proliferation). (M–Q) HFB spheroids display different gene expression and activity profiles based on their diameter on qPCR analysis at day 7. Fibroblasts in spheroid form showed significantly higher expression levels of fibrosis genes (αSMA and collagen-1) versus 2D monolayer-cultured cells. Among spheroids, 200 μm showed the highest expression levels of fibrosis genes and lower expression levels of matrix metalloproteinase genes (MMP1, MMP2, MMP7). M, Mono-layer cultured fibroblast as control; 100, 200, 300 represent the spheroid diameter of each group. ($n = 3$; $*p < 0.05$). Scale bars: (A–C) = 100 μm ; (G–I) = 100 μm ; (J–L) = 50 μm .

distributed in the core part than peripheral regions. More interestingly, the hybrid spheroids with lower macrophage ratios (16 : 1, 32 : 1 and 64 : 1) showed higher levels and more homogeneous distribution of both collagen-1 and collagen-3 deposition compared to the other groups (Fig. 6B and C). As was seen with qPCR analysis, F16 hybrid spheroids consistently had the highest collagen deposition and distribution among all groups.

Discussion

The classical *in vitro* model of fibrogenesis is mainly focused on culture in a 2D monolayer.⁴ However, cells cultured in a 2D environment behave fundamentally differently from cells *in vivo* with regard to both physiology and cellular response. These differences have prevented better mechanistic understanding of the processes underlying fibrosis as well as exploration of potential interventions. For example, it is known that for implanted objects, the fibrosis response is dependent on many factors – size, geometric shape, porosity, material, mechanical stiffness, and many others.^{6,32} It is impossible to explore all of these possible variables – each of which has con-

foundering interaction effects with other variables – in animals to understand how they interact or to what extent different pathways are involved. A more realistic *in vitro* model is therefore of great importance.

Mounting evidence indicates that 3D spheroids are a more representative model of the *in vivo* environment, promoting cell–cell interactions and communication.¹¹ We propose that 3D spheroids can fill the gap between conventional 2D cell culture and animal models to accelerate translational research in tissue engineering and fibrosis research.³³

Our data shows that human fibroblasts in 3D spheroid form had significantly higher expression levels of fibrosis genes (αSMA and *Col1a1*) compared to 2D monolayer culture, which indicates that fibroblast-only spheroids do display different behavior even without immune cell presence. Creation of fibroblast-only spheroids from human skin has only recently been described.³⁴ Interestingly, in that report fibroblasts in spheroid form were less active, though it appears to be because the fibroblasts began in an aggressive myofibroblast phenotype which then reverted over time when in spheroids but not when in monolayer. Both mechanical stress and TGF- β can cause differentiation to myofibroblasts.³⁵ In our study, we began with fibroblasts

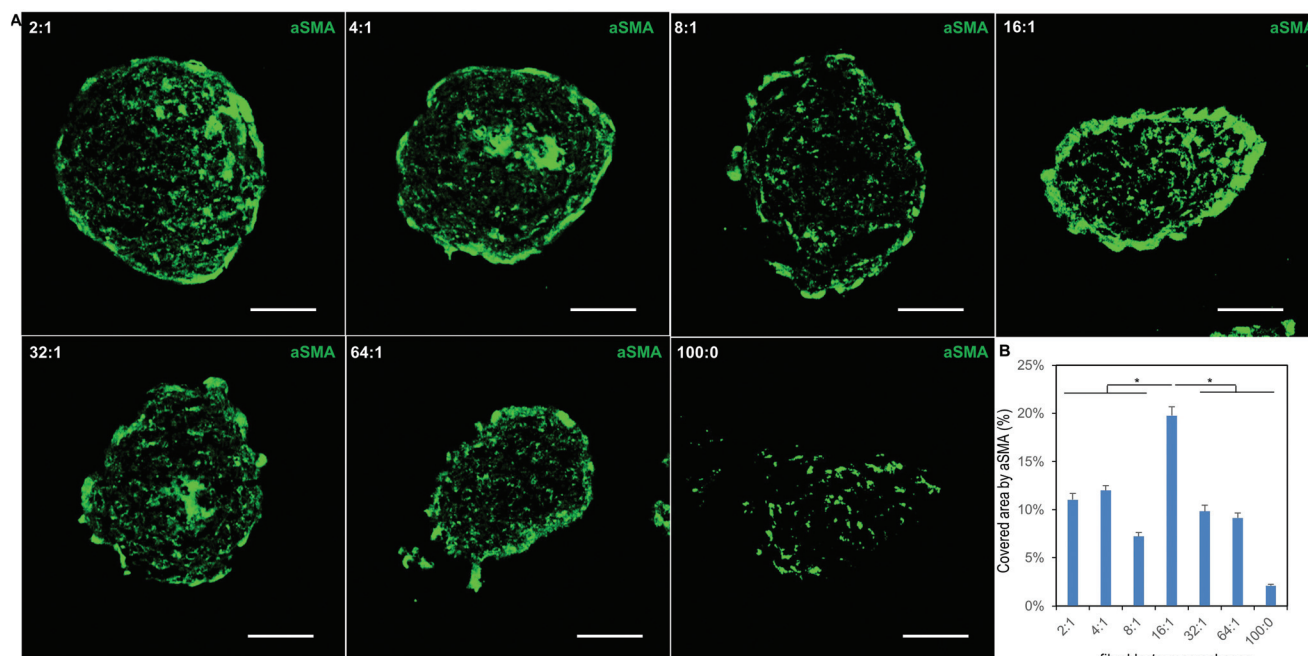


Fig. 3 Single channel images from immunofluorescent staining of hybrid spheroids with activated fibroblast marker. (A) Confocal images of frozen sections of hybrid spheroids (fibroblasts to macrophages from 2 : 1, 4 : 1, 8 : 1, 16 : 1, 32 : 1, 64 : 1 and 100 : 0) stained with aSMA. aSMA is activated fibroblast (myofibroblast) marker, scale bars: 50 μ m. (B) Semi-quantification of confocal images for aSMA ($n = 3$; * $p < 0.05$).

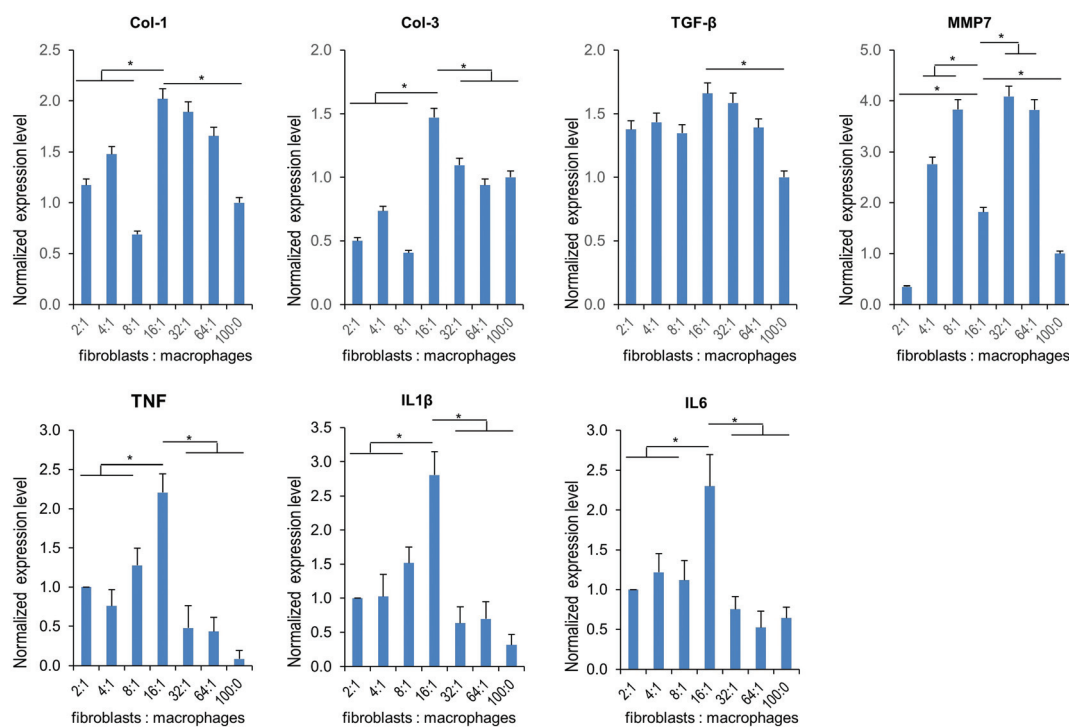


Fig. 4 Hybrid macrophage-fibroblast spheroids display different qPCR gene expression profiles based on the ratio of macrophages present in the spheroid. Quantitative PCR analysis of hybrid spheroids containing fibroblast and macrophages across differing ratios at day 7. Relative expression levels of fibrosis related genes (Col-1, Col-3, and TGF- β), matrix metalloproteinase gene (MMP7) and inflammation related genes (TNF, IL1 β and IL6) ($n = 3$; * $p < 0.05$).

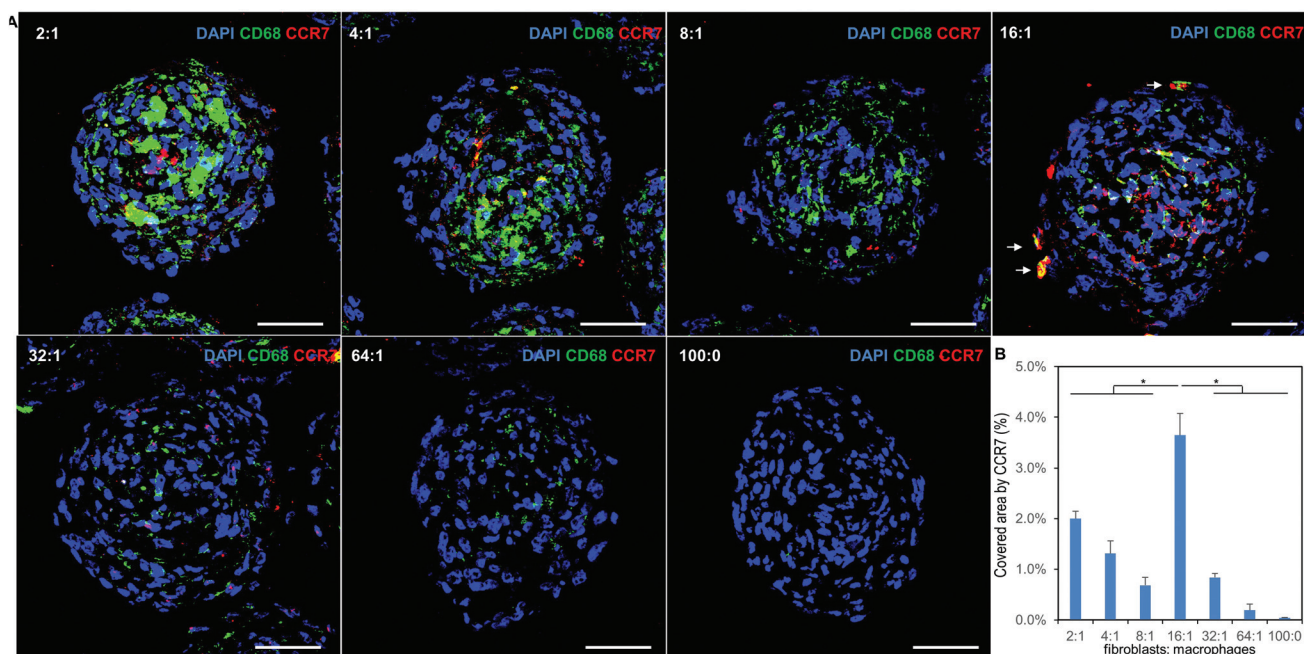


Fig. 5 F16 ratio hybrid spheroids demonstrate increased pro-fibrotic macrophage activity on immunofluorescent staining. (A) Confocal images of hybrid spheroid frozen sections (fibroblast to macrophage ratios 2 : 1, 4 : 1, 8 : 1, 16 : 1, 32 : 1, 64 : 1 and 100 : 0) stained with CD68 and CCR7 (M1-phenotype macrophage marker). White arrows indicate CD86+ macrophages in the F16 spheroid that have polarized toward an M1 phenotype. (b) Semi-quantification of confocal images for CCR7. ($n = 3$; $*p < 0.05$). Scale bars: 50 μm .

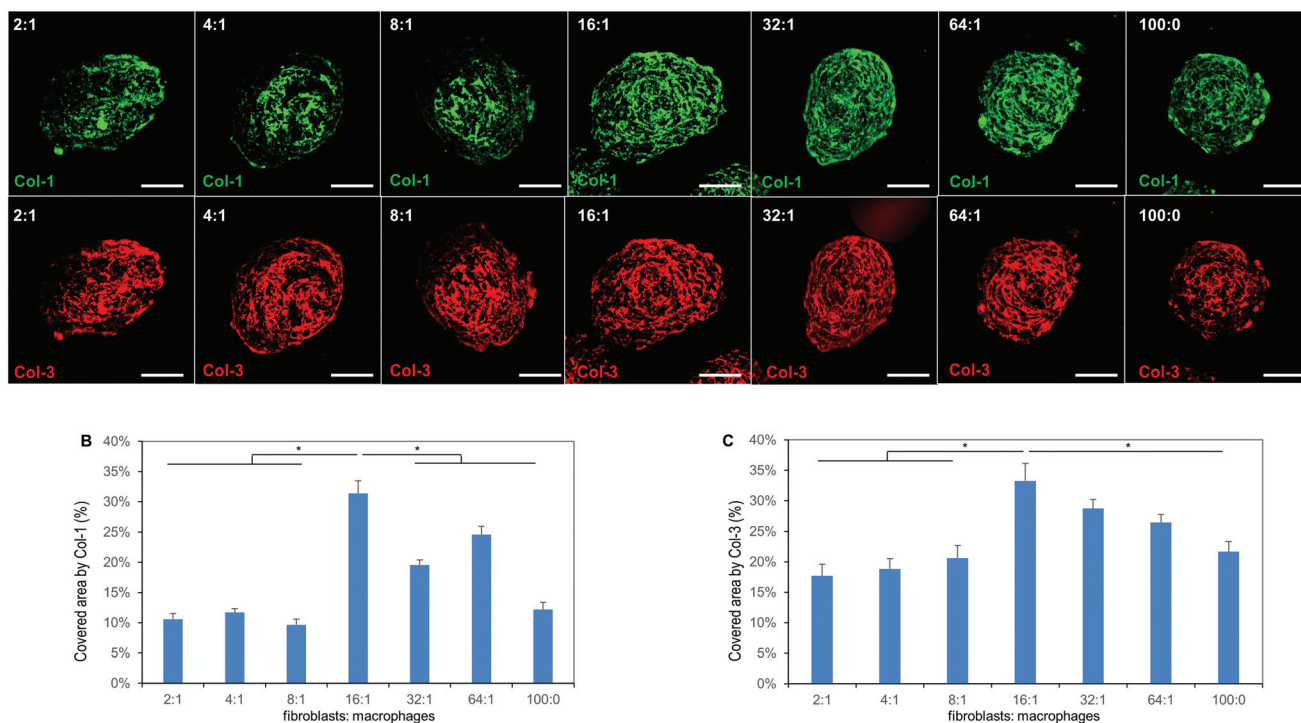


Fig. 6 Hybrid spheroids demonstrate macrophage ratio-dependent collagen deposition. (A) Confocal images of hybrid spheroid frozen sections (fibroblasts to macrophages from 2 : 1, 4 : 1, 8 : 1, 16 : 1, 32 : 1, 64 : 1 and 100 : 0) stained with collagen-1 and collagen-3 respectively. 16 : 1 ratio hybrid spheroids showed higher levels and more homogeneous distribution of both collagen-1 and collagen-3 deposition on immunofluorescent stain. Scale bars: 50 μm . (B–C) Semi-quantification of confocal images for Col-1 and Col-3. ($n = 3$; $*p < 0.05$). Scale bars: 50 μm .

displaying standard morphology for both spheroids and monolayers.

The size of diffusion-dependent spheroids plays a key role in their function and viability due to the hypoxia conditions developed as the gradient of oxygen progresses from normoxia at the periphery to hypoxia at the core.³⁶ Thus, in the larger spheroids, the supply of nutrients and oxygen to the cells is insufficient to maintain cellular viability and normal function. Previous studies have shown that spheroids with a diameter over 500 μm develop an apoptotic or necrotic core over time.³⁷ Therefore, 500 μm in diameter was chosen as the upper limit of spheroid size in this study. However, if the spheroid is too small, the beneficial effects of cell–cell interaction over 2D culture will diminish. A lower limit of 100 μm was applied because spheroids under this size are more like multiple cellular clusters rather than 3D microtissue. In addition, spheroids less than 100 μm in diameter are challenging for processing and sectioning for histology analysis. Therefore, our research mainly focused on optimization regarding the size of spheroids within the range of 100 to 500 μm in diameter.

Our data showed significant cell apoptosis occurred in spheroids with larger size (400 and 500 μm in diameter). The level of hypoxia in the spheroids was promoted by the abundant deposition of dense collagen 1 fibers at the periphery of the spheroids (Fig. 1A–E), which may have further limited inward nutrient diffusion and outward egress of metabolites from the spheroid center. Our data suggested that spheroids with a 200 μm diameter represent the best balance between diffusion and 3D behavior, leading to more homogeneity, abundant collagen-1 deposits in the ECM, and significantly higher expression levels of fibrosis genes (αSMA and collagen-1) compared to the spheroids with 100 and 300 μm diameters. We therefore adopted 200 μm as the optimal spheroid diameter for further research.

It is well known that macrophages play a central role in inflammation and the subsequent development of fibrosis in a range of organ pathologies.¹⁸ For this reason, macrophage/fibroblast co-culture in a 2D monolayer has been recently described to investigate the inflammatory effects of biomaterials.^{38,39} However, as previously mentioned, monolayer models have consistently demonstrated limited predictive value for the 3D *in vivo* environment and these shortcomings are exacerbated when cell-material surface interactions are of paramount importance.⁴

We felt that spheroids composed of the key cell lineages in the fibrosis process (fibroblasts and macrophages) would offer a model displaying the closest behavior to an *in vivo* setting. To evaluate this, macrophages were added to the spheroids in different ratios (fibroblast : macrophage: 2 : 1, 4 : 1, 8 : 1, 16 : 1, 32 : 1, 64 : 1 and 100% fibroblast as control). Even higher concentrations of macrophages (1 : 1 and 1 : 2 fibroblast : macrophage) failed to form spheroids, likely due to inadequate ECM secretion to support aggregation. Concentrations lower than 1 : 64 (1 : 128, *etc.*) were expected to have too few macrophages present to show a difference *versus* the fibroblast-only spheroid group. Our aim was to cover a range of macrophage

concentrations from the highest possible concentration that would support spheroid formation to a concentration low enough that similarity to fibroblast-only spheroids was likely.

Our immunofluorescent staining indicated the addition of macrophages to the spheroids enhanced collagen-1 maturation (HSP47), which could be explained by the paracrine effects of macrophages on the fibroblasts. Previous literature shows fibroblast activity is largely mediated by macrophage-generated signals to produce more collagen during the fibrogenesis process.^{40–42}

Our data showed that too few macrophages (32 : 1 and 64 : 1) in the spheroids limited the macrophage-induced paracrine effects, with less cytokine secretion ultimately leading to less collagen deposition by the fibroblasts. The reason for less fibrogenesis in high-macrophage spheroids (2 : 1, 4 : 1 and 8 : 1) is less clear. Regions of dense CD68-positive activity were seen (ESI Fig. 3†) which may represent giant cells formed by multiple macrophages or clusters of macrophages in close proximity.⁴³ While further investigation is necessary to explore this phenomenon, these dense areas of CD68 were correlated with less fibroblast activity and presumably a less desirable fibrosis microtissue model. The qPCR data was also consistent with IF staining and further confirmed that the hybrid spheroids with fibroblasts and macrophages at a 16 : 1 ratio had the highest expression levels of fibrosis-related genes (Col-1a1, Col-3a1 and TGF- β).⁴⁴

In prior work, we have combined scaffold-free spheroid systems with nano-materials in cardiac tissue engineering and plan to do the same with this model.^{28,45} Future work will also include efforts to modulate cell activity using exogenous signalling molecules and other methods to perturb the system.

Interestingly, despite a greater total number of macrophages being present in the 2 : 1, 4 : 1, and 8 : 1 hybrid spheroids (ESI Fig. 3 and 4A†), the greatest amount of CCR7-positive, M1-phenotype macrophage activity by far was in the 16 : 1 group (Fig. 5). The 32 : 1 and 64 : 1 hybrid spheroids also displayed little M1 activity, suggesting that greater M1 polarization may be an underlying mechanism by which the observed pro-fibrotic effects in the F16 group are mediated.

While the ratio of fibroblasts to macrophages during fibrogenesis has not been conclusively studied and varies based on tissue type and other factors, within a given site it is clearly dynamic over time. Based on the limited available data, in a mouse myocardial infarction model a ratio of 16 : 1 represents the beginnings of the subacute stage of fibrogenesis at post-event day 28, while 4 : 1 is most like the early state from day 7 to 14 when collagen accumulation begins.⁴⁶ Future studies will explore the interesting question of whether macrophage ratio can be manipulated to generate models that simulate earlier or later time points in the fibrosis process.

We also investigated how the cell phenotype changes with hybrid spheroids, in the form of fibroblast activation and macrophage polarization. Our data indicates that significantly more fibroblasts become activated to myofibroblasts in F16 spheroids as indicated by higher expression levels of αSMA . Similarly, more macrophages were polarized towards a pro-

inflammatory type M1 in this group with greater CCR7 and pSTAT1 expression. This finding suggests that the optimal ratio permits a more effective paracrine effect between macrophages and fibroblasts to drive the balance between pro- and anti-fibrosis towards a more pro-fibrotic environment.^{47,48}

Fibrogenesis models are typically characterized based on ECM synthesis, particularly collagen-1 and collagen-3.⁴⁹ Our IF data indicates the F16 ratio hybrid spheroids had more homogeneous distribution and greater quantities of both collagen-1 and collagen-3 deposition compared to the other groups. These spheroids showed the highest expression levels of fibrosis-related genes (*Col-1a1*, *Col-3a1* and *TGF-β*) and inflammation-related genes (*TNF*, *IL1β* and *IL6*) among all the groups, with a lower expression level of fibrolytic *MMP7*. *MMP-7* has been shown to have both pro- and anti-fibrotic activity, depending on the stage of wound healing, and is an intriguing marker for exploring the spheroid model in future mechanistic studies.⁵⁰

One mechanistic hypothesis for the superiority of the F16 group over other macrophage concentrations may relate to the possibility that sixteen fibroblasts localized around one macrophage represent an ideal spatial distribution for cell-cell contact. The reason for substantially higher fibrosis in the F16 group compared to lower macrophage concentrations, even 32:1, is less clear, but may simply relate to less total macrophage presence resulting in lower concentrations of pro-inflammatory signals. Regardless of mechanism, the 16:1 ratio in hybrid fibroblast-macrophage spheroids consistently appears to balance effector fibroblasts and regulating macrophages to achieve higher levels of fibrosis and a more homogeneous deposition of collagen.

Conclusions

We have developed and optimized the first “fibrosis spheroid”: a scaffold-free three-dimensional human fibroblast-macrophage spheroid microtissue system. We demonstrated high cell viability and abundant collagen deposition for an *in vitro* fibrosis model, with an ideal diameter of 200 μm. The optimized 16:1 spheroid model showed higher collagen 1 and 3 gene expression, greater αSMA and collagen deposition and a significantly increased degree of collagen maturation *versus* either standard 2D monolayer cultures or 3D fibroblast-only spheroids. The degree of M1 macrophage polarization appears to be a contributing mechanistic factor in the model, with the 16:1 ratio showing both the most fibrosis and the highest M1 macrophage activity. Future work will focus on evaluation of this system as an *in vitro* fibrogenesis model for high-throughput anti-fibrosis therapy screening and evaluation of material biocompatibility.

Conflicts of interest

There are no conflicts to declare.

Acknowledgements

The authors would like to acknowledge Ms. Melissa Noyes for assistance with data collation and manuscript preparation and thank Drs Dacheng Ding and Alexander Hillel for providing primary human fibroblasts. The work is supported by the start-up funds from Johns Hopkins University (D. C.). This study used the services of core grant EY001765 from NIH.

Notes and references

- 1 A. Birbrair, T. Zhang, D. C. Files, S. Mannava, T. Smith, Z.-M. Wang, M. L. Messi, A. Mintz and O. Delbono, *Stem Cell Res. Ther.*, 2014, DOI: 10.1186/scrt512.
- 2 S. L. Friedman, D. Sheppard, J. S. Duffield and S. Violette, *Sci. Transl. Med.*, 2013, **5**, 167sr1.
- 3 T. A. Wynn, *Nat. Rev. Immunol.*, 2004, **4**, 583–594.
- 4 C. Z. Chen and M. Raghunath, *Fibrog. Tissue Repair*, 2009, **2**, 7.
- 5 N. X. Landén, D. Li and M. Ståhle, *Cell. Mol. Life Sci.*, 2016, **73**, 3861–3885.
- 6 J. C. Doloff, O. Veisheh, A. J. Vegas, H. H. Tam, S. Farah, M. Ma, J. Li, A. Bader, A. Chiu, A. Sadraei, S. Aresta-Dasilva, M. Griffin, S. Jhunjunwala, M. Webber, S. Siebert, K. Tang, M. Chen, E. Langan, N. Dholokia, R. Thakrar, M. Qi, J. Oberholzer, D. L. Greiner, R. Langer and D. G. Anderson, *Nat. Mater.*, 2017, **16**, 671–680.
- 7 J. M. Anderson, A. Rodriguez and D. T. Chang, *Semin. Immunol.*, 2008, **20**, 86–100.
- 8 L. Chung, D. R. Maestas, F. Housseau and J. H. Elisseeff, *Adv. Drug Delivery Rev.*, 2017, **114**, 184–192.
- 9 T. A. Wynn and T. R. Ramalingam, *Nat. Med.*, 2012, **18**, 1028–1040.
- 10 Q. Xu, J. T. Norman, S. Shrivastav, J. Lucio-Cazana and J. B. Kopp, *Am. J. Physiol.: Renal, Fluid Electrolyte Physiol.*, 2007, **293**, F631–F640.
- 11 E. Fennema, N. Rivron, J. Rouwkema, C. van Blitterswijk and J. de Boer, *Trends Biotechnol.*, 2013, **31**, 108–115.
- 12 T. Ishiguro, H. Ohata, A. Sato, K. Yamawaki, T. Enomoto and K. Okamoto, *Cancer Sci.*, 2017, **108**, 283–289.
- 13 T.-M. Achilli, J. Meyer and J. R. Morgan, *Expert Opin. Biol. Ther.*, 2012, **12**, 1347–1360.
- 14 P. Salmenperä, P.-R. Karhemo, K. Räsänen, P. Laakkonen and A. Vaheri, *Exp. Cell Res.*, 2016, **345**, 17–24.
- 15 C. S. Ong, T. Fukunishi, H. Zhang, C. Y. Huang, A. Nashed, A. Blazeski, D. DiSilvestre, L. Vricella, J. Conte, L. Tung, G. F. Tomaselli and N. Hibino, *Sci. Rep.*, 2017, **7**, 4566.
- 16 K. R. Silva, R. A. Rezende, F. D. A. S. Pereira, P. Gruber, M. P. Stuart, A. Ovsianikov, K. Brakke, V. Kasyanov, J. V. L. da Silva, J. M. Granjeiro, L. S. Baptista and V. Mironov, *PLoS One*, 2016, **11**, e0166073.
- 17 M. W. Laschke and M. D. Menger, *Trends Biotechnol.*, 2017, **35**, 133–144.
- 18 T. A. Wynn and L. Barron, *Semin. Liver Dis.*, 2010, **30**, 245–257.

- 19 A. Falkenham, R. de Antueno, N. Rosin, D. Betsch, T. D. G. Lee, R. Duncan and J.-F. L egar e, *Am. J. Pathol.*, 2015, **185**, 927–942.
- 20 J. Barthes, C. Dollinger, C. B. Muller, U. Liivas, A. Dupret-Bories, H. Knopf-Marques and N. E. Vrana, *Front. Bioeng. Biotechnol.*, 2018, **6**, 108.
- 21 E. M. Moore, G. Ying and J. L. West, *Adv. Biosyst.*, 2017, **1**, 1600021.
- 22 L. Zhao, M. Shi, Y. Liu, X. Zheng, J. Xiu, Y. Liu, L. Tian, H. Wang, M. Zhang and X. Zhang, *Anal. Chem.*, 2019, **91**, 4307–4311.
- 23 D. R. Namba, G. Ma, I. Samad, D. Ding, V. Pandian, J. D. Powell, M. R. Horton and A. T. Hillel, *Otolaryngol.–Head Neck Surg.*, 2015, **152**, 881–888.
- 24 S. Eligini, M. Crisci, E. Bono, P. Songia, E. Tremoli, G. I. Colombo and S. Colli, *J. Cell. Physiol.*, 2013, **228**, 1464–1472.
- 25 A. Tallam, T. M. Perumal, P. M. Antony, C. J ager, J. V. Fritz, L. Vallar, R. Balling, A. del Sol and A. Michelucci, *PLoS One*, 2016, DOI: 10.1371/journal.pone.0149050.
- 26 J. Q. Davies and S. Gordon, in *Basic Cell Culture Protocols*, ed. C. D. Helgason and C. L. Miller, Humana Press, Totowa, NJ, 2005, pp. 105–116.
- 27 M. Saghaeian-Jazi, S. Mohammadi and S. Sedighi, *Zahedan J. Res. Med. Sci.*, 2016, **18**(6), e7362.
- 28 Y. Tan, D. Richards, R. C. Coyle, J. Yao, R. Xu, W. Gou, H. Wang, D. R. Menick, B. Tian and Y. Mei, *Acta Biomater.*, 2017, **51**, 495–504.
- 29 K. J. Livak and T. D. Schmittgen, *Methods*, 2001, **25**, 402–408.
- 30 X. Li, B. Cho, R. Martin, M. Seu, C. Zhang, Z. Zhou, J. S. Choi, X. Jiang, L. Chen, G. Walia, J. Yan, M. Callanan, H. Liu, K. Colbert, J. Morrissette-McAlmon, W. Grayson, S. Reddy, J. M. Sacks and H.-Q. Mao, *Sci. Transl. Med.*, 2019, **11**, eaau6210.
- 31 F. Raggi, S. Pelassa, D. Pierobon, F. Penco, M. Gattorno, F. Novelli, A. Eva, L. Varesio, M. Giovarelli and M. C. Bosco, *Front. Immunol.*, 2017, DOI: 10.3389/fimmu.2017.01097.
- 32 B. F. Matlaga, L. P. Yasenachak and T. N. Salthouse, *J. Biomed. Mater. Res.*, 1976, **10**, 391–397.
- 33 K. M. Yamada and E. Cukierman, *Cell*, 2007, **130**, 601–610.
- 34 G. Granato, M. R. Ruocco, A. Iaccarino, S. Masone, G. Cali, A. Avagliano, V. Russo, C. Bellevicine, G. Di Spigna, G. Fiume, S. Montagnani and A. Arcucci, *Cell Death Discovery*, 2017, **3**, 17038.
- 35 B. Hinz, S. H. Phan, V. J. Thannickal, A. Galli, M.-L. Bochaton-Piallat and G. Gabbiani, *Am. J. Pathol.*, 2007, **170**, 1807–1816.
- 36 I. Dufau, C. Frongia, F. Sicard, L. Dedieu, P. Cordelier, F. Ausseil, B. Ducommun and A. Valette, *BMC Cancer*, 2012, **12**, 15.
- 37 T. J. Bartosh, J. H. Yl ostalo, A. Mohammadipoor, N. Bazhanov, K. Coble, K. Claypool, R. H. Lee, H. Choi and D. J. Prockop, *Proc. Natl. Acad. Sci. U. S. A.*, 2010, **107**, 13724–13729.
- 38 G. Zhou, H. Loppnow and T. Groth, *Acta Biomater.*, 2015, **26**, 54–63.
- 39 H. Pan, H. Jiang, S. Kantharia and W. Chen, *Biomed. Mater.*, 2011, **6**, 065002.
- 40 G. Westergren-Thorsson, K. Larsen, K. Nihlberg, A. Andersson-Sj oland, O. Hallgren, G. Marko-Varga and L. Bjermer, *Clin. Respir. J.*, 2010, **4**, 1–8.
- 41 *The Macrophage*, ed. B. Burke, C. E. Lewis, Oxford University Press, 2002, <https://global.oup.com/academic/product/the-macrophage-9780192631978?cc=us&lang=en&>, (accessed March 8, 2019).
- 42 E. Solheim, B. Sudmann, G. Bang and E. Sudmann, *J. Biomed. Mater. Res.*, 2000, **49**, 257–263.
- 43 Y. Zhu, C. M. Sk old, X. Liu, H. Wang, T. Kohyama, F. Q. Wen, R. F. Ertl and S. I. Rennard, *Respir. Res.*, 2001, **2**, 295–299.
- 44 A. M. Manicone, I. Huizar and J. K. McGuire, *Am. J. Pathol.*, 2009, **175**, 2319–2331.
- 45 Y. Tan, D. Richards, R. Xu, S. Stewart-Clark, S. K. Mani, T. K. Borg, D. R. Menick, B. Tian and Y. Mei, *Nano Lett.*, 2015, **15**, 2765–2772.
- 46 Y.-F. Jin, H.-C. Han, J. Berger, Q. Dai and M. L. Lindsey, *BMC Syst. Biol.*, 2011, **5**, 60.
- 47 D. T. Luttkhuizen, M. C. Harmsen and M. J. A. Van Luyn, *Tissue Eng.*, 2006, **12**, 1955–1970.
- 48 D. J. Holt, L. M. Chamberlain and D. W. Grainger, *Biomaterials*, 2010, **31**, 9382–9394.
- 49 A. M. Porras, H. N. Hutson, A. J. Berger and K. S. Masters, *Curr. Opin. Biotechnol.*, 2016, **40**, 24–30.
- 50 M. Giannandrea and W. C. Parks, *Dis. Models Mech.*, 2014, **7**, 193–203.